4

Minority Carriers and Thermoelectric Effects in Bipolar Devices

Kevin Pipe
University of Michigan

4.1 Introduction

Discussion of thermoelectric effects has until now been mostly restricted to the context of majority carriers; that is, electron flow in n-type materials and hole flow in p-type materials. While conventional thermoelectric devices are typically unipolar and have negligible transport by minority carriers, there are important bipolar devices for which the presence of holes in n-type materials, or electrons in p-type materials, plays a crucial role in current and heat flow.

For the broad class of active electronics and optoelectronics, which includes devices like bipolar transistors, diodes, semiconductor lasers, and optical amplifiers, the injection of minority carriers is basic to operation. As these devices shrink smaller in size through integration and must dissipate heat into considerably smaller surrounding space, thermal management assumes an increasingly high priority. This is especially relevant for many modern devices which are based on alloys or superlattices with low thermal conductivities. In cooling such microscale devices, conventional large-area Peltier coolers can be quite inefficient, prompting the study of thermoelectrics at small size scales.

Two ways to implement thermoelectric cooling for an active electronic or optoelectronic device are to fabricate a microscale thin-film cooler near the device which cools it externally or to examine the active device structure to optimize its thermoelectric properties and create internal cooling. This chapter will cover the latter approach, extending the conventional thermoelectric description to encompass transport in active devices and leaving the former approach for discussions in other chapters.

To arrive at a generalized technique for the study of thermoelectric effects in bipolar devices, the presence of majority and minority carriers must be considered. In this chapter, transport in a conventional Peltier cooler (where minority-carrier effects are minimal) has been considered, followed by an introduction of the bipolar Peltier coefficient and examination of the effects of minority carriers on the thermoelectric properties of fundamental active structures such as the p–n junction.

4.2 Conventional Thermoelectric Cooler

The conventional Peltier cooler, described in Chapter 1, is electrically equivalent to an alternating series of n-type and p-type resistors, which are connected by metal contacts. As voltage is applied across the cooler, a drift current density develops within each resistor which is proportional to the free carrier concentrations and carrier mobilities:

$$J_{\text{tot}} = J_{\text{e}} + J_{\text{h}} = (\sigma_{\text{e}} + \sigma_{\text{h}})\varepsilon = (n\mu_{\text{e}} + p\mu_{\text{h}})e\varepsilon \tag{4.1}$$

where σ_{e} and σ_{h} are electrical conductivities, μ_{e} and μ_{h} are carrier mobilities, n and p are carrier concentrations, ε is the component of the applied electric field in the direction of current flow, and e is the unit electric charge. In n-type regions (where $n >> p$), the current is carried almost entirely by electrons, while in p-type regions it is carried almost entirely by holes.

At equilibrium, when no voltage is applied across the cooler and no net current is flowing, the Fermi energy is constant throughout the device, as shown in Figure 4.1b. This leads to an offset in the average transport energy of free carriers, at each metal–semiconductor junction, as carriers in the metal are distributed nearly symmetrically around the Fermi level and those in the semiconductor are constrained to lie beyond the band edge. As electrical bias is applied as shown in Figure 4.1c. and current flows through the cooler, carriers move between near-equilibrium distributions on either side of each junction and exchange heat energy with the surrounding lattice to compensate for the energy offsets. This heat exchange is described by the thermoelectric Peltier effect, which defines a Peltier coefficient π for each material such that an interface energy offset is given by $e\Delta\pi$.

4.3 Bipolar Peltier Coefficient

The total Peltier coefficient which accounts for transport by both electrons and holes can be derived according to the steady-state Boltzmann transport equation, using the relaxation time approximation and is given by[1]:

$$\pi = \frac{1}{e}\frac{\dfrac{\mu_{\text{e}}}{\tau_{\text{e}}}[(E_{\text{F}} - E_{\text{C}})I_{1\text{e}} - I_{2\text{e}}] - \dfrac{\mu_{\text{h}}}{\tau_{\text{h}}}[(E_{\text{V}} - E_{\text{F}})I_{1\text{h}} - I_{2\text{h}}]}{\dfrac{\mu_{\text{e}}}{\tau_{\text{e}}}I_{1\text{e}} + \dfrac{\mu_{\text{h}}}{\tau_{\text{h}}}I_{1\text{h}}} \tag{4.2}$$

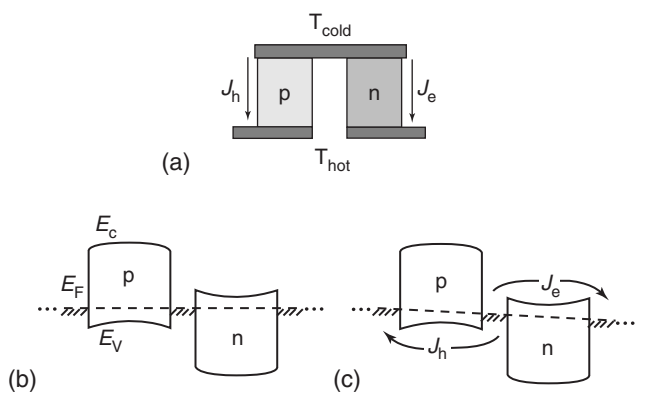

FIGURE 4.1 Conventional Peltier cooler: (a) physical structure; (b) unbiased band structure; and (c) biased band structure. Note that $J_{\text{h}} \approx J_{\text{e}}$ (minority currents are negligible).

where

$$I_{se} = \frac{2m_e^{*^2}}{\hbar^4}\int_{E_C}^{\infty}\frac{\partial f_{oe}}{\partial E}(E-E_C)^{r+s}\,dE \tag{4.3a}$$

$$I_{sh} = \frac{2m_h^{*^2}}{\hbar^4}\int_{-\infty}^{E_V}\frac{\partial f_{oh}}{\partial E}(E_V-E)^{r+s}\,dE \tag{4.3b}$$

τ_e and τ_h are relaxation times for electrons and holes, respectively; m_e^* and m_h^* are effective masses; f_{oe} and f_{oh} are equilibrium Fermi–Dirac distributions, and $r \approx r_e \approx r_h$ is the scattering parameter defined in terms of the mean free path λ by $\lambda \propto (E-E_C)^r$. Note that $r = 1/2$ for optical phonon scattering (dominant in III–V semiconductors) at temperatures less than the Debye temperature.

In the case for which the electron concentration is large and E_F is much closer to E_C than E_V, the total Peltier coefficient given in Equation 4.2 can be reduced to the electron component:

$$\pi_e = -\frac{1}{e}\frac{\int_{E_C}^{\infty}(E-E_C)^{r+1}(E-E_F)\left(-\frac{\partial f_{oe}}{\partial E}\right)dE}{\int_{E_C}^{\infty}(E-E_C)^{r+1}\left(-\frac{\partial f_{oe}}{\partial E}\right)dE} = -\frac{1}{e}\frac{\int_{E_C}^{\infty}\sigma_e'(E)(E-E_F)\left(-\frac{\partial f_{oe}}{\partial E}\right)dE}{\int_{E_C}^{\infty}\sigma_e'(E)\left(-\frac{\partial f_{oe}}{\partial E}\right)dE} \tag{4.4}$$

where the "differential" conductivity $\sigma_e'(E)$ has been introduced, giving the contribution of an electron at energy E to the overall conductivity in terms of the average electron velocity $\bar{v}_x(E)$ and density $\bar{n}(E)$ through[2,3]

$$\sigma_e'(E) \equiv e^2\tau_e(E)\int\int v_x^2(E,k_y,k_z)dk_y\,dk_z \approx e^2\tau_e(E)\bar{v}_x^2(E)\bar{n}(E) \tag{4.5}$$

An analogues expression defining π_h can be written for the case in which the hole concentration is large and E_F is much closer to E_V than E_C:

$$\pi_h = \frac{1}{e}\frac{\int_{-\infty}^{E_V}(E_V-E)^{r+1}(E_F-E)\left(-\frac{\partial f_{oh}}{\partial E}\right)dE}{\int_{-\infty}^{E_V}(E_V-E)^{r+1}\left(-\frac{\partial f_{oh}}{\partial E}\right)dE} = \frac{1}{e}\frac{\int_{-\infty}^{E_V}\sigma_h'(E)(E_F-E)\left(-\frac{\partial f_{oh}}{\partial E}\right)dE}{\int_{-\infty}^{E_V}\sigma_h'(E)\left(-\frac{\partial f_{oh}}{\partial E}\right)dE} \tag{4.6}$$

From Equation 4.4 and Equation 4.6 it is apparent that $|\pi_e|$ and $|\pi_h|$ increase as the carrier distribution becomes more asymmetric with respect to the Fermi energy, since $\frac{\partial f_o}{\partial E}$ is sharply peaked near E_F. The magnitude of the Peltier coefficient has an inverse relationship with carrier concentration (as shown in Figure 4.2), since decreasing doping moves the Fermi energy further into the bandgap while the carriers are constrained to stay in the bands. For high carrier concentrations, such as those found in metals, the Peltier coefficient is approximately zero.

The cooling power density at the center (cold) contact of the biased conventional Peltier cooler in Figure 4.1c. is given by

$$Q_{conv} = J_h\pi_{p,h} - J_e\pi_{n,e} = J(\pi_{p,h} - \pi_{n,e}) \tag{4.7}$$

where J_h and J_e are both taken to be positive and $\pi_{p,h}$ refers to the Peltier coefficient of holes in the p-type region. Since the Fermi level is near the valence band in the p-type region, holes which enter the semiconductor from the center metal contact experience only a slight increase in energy; the Peltier coefficient $\pi_{p,h}$ for these majority carriers is small. The Peltier coefficient $\pi_{p,e}$ for minority carriers is much larger; if electrons were to be injected into the p-type region from the center contact, these would pull much more heat out of the lattice. The same is true for holes injected into the n-type region.

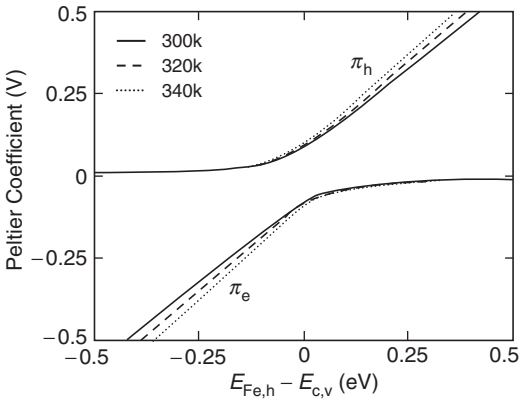

FIGURE 4.2 Variation of the Peltier coefficient components in GaAs (π_e for electrons and π_h for holes) with Fermi energy and hence with carrier concentration.

This process of minority carrier injection is fundamental to the operation of most active devices. The application of thermoelectric theory to such devices begins with a description of the transport of minority carriers.

4.4 Minority Carriers and Quasi-Fermi Levels

When a device is unbiased, electron and hole populations are in equilibrium with each other as well as with the semiconductor lattice, and a single Fermi level can be used to characterize the distribution of carriers. As voltage is applied and the device moves out of equilibrium, there is a net motion of carriers, and the distribution functions of electrons and holes are altered. The nonequilibrium description which is often used is an approximation of each carrier population by a Fermi–Dirac distribution at the lattice temperature, defining separate quasi-Fermi levels E_{Fe} and E_{Fh} for electrons and holes, respectively.[4,5] This reflects the assumptions that very fast carrier-phonon scattering leads to electron-lattice and hole-lattice thermal equilibrium and that the generation and recombination processes governing transitions between the electron and hole populations are too slow to bring these two species to equilibrium.

For the conventional Peltier cooler, electrically equivalent to a series of resistors, transport is dominated by the drift of majority carriers. Because concentrations of majority and minority carriers change very little when the device is biased, the quasi-Fermi levels for electrons and holes do not split apart and remain at the equilibrium position in the bandgap, tilting to reflect current flow as shown in Figure 4.1c.

For active electronic devices as fundamental as the p–n diode, on the other hand, transport is dominated by the diffusion of minority carriers. When voltage bias is applied to the diode, the minority carrier concentrations on either side of the p–n junction grow by orders of magnitude above their equilibrium amounts, causing diffusion currents to flow as well as causing the splitting of the quasi-Fermi levels as illustrated in Figure 4.3c.[6]

4.5 Thermoelectric Cooling in Bipolar Devices

The p–n junction which constitutes a bipolar diode is a basic building-block of most active devices. In order to quantify the thermoelectric behavior of devices, in which transport is governed by majority and minority carriers, the forms of the Peltier coefficient given above are used to separate

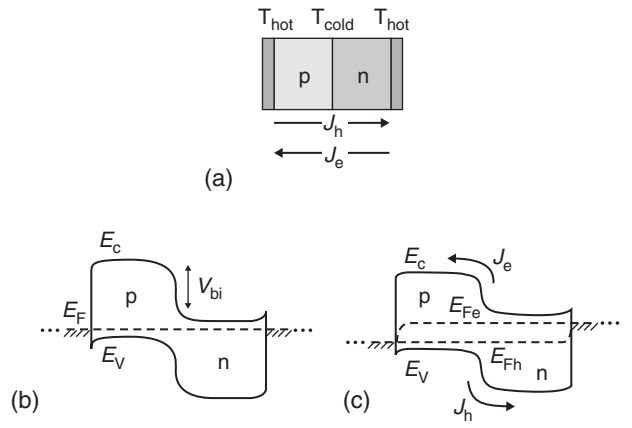

FIGURE 4.3 p–n diode: (a) physical structure; (b) unbiased band structure; and (c) biased band structure showing quasi-Fermi level splitting.

transport into electron and hole components. Within each region there is a coefficient π_e for electrons and a coefficient π_h for holes which are defined not in terms of a common Fermi level E_F but rather in terms of the quasi-Fermi levels E_{Fe} and E_{Fh}, respectively. The majority carrier coefficient remains nearly at its equilibrium value, but the minority carrier coefficient changes dramatically as the minority carrier concentration changes. The horizontal axis on Figure 4.2 is interpreted to be the distance between the quasi-Fermi level and band edge, which decreases for minority carriers as the bias increases and more such carriers are injected. Because the minority carrier concentration is tied to the device bias level, the minority carrier Peltier coefficient is *bias-dependent*.[7]

The thermoelectric behavior of the p–n junction is analyzed first, and it is later shown how this method can be applied to more complicated structures. This discussion will focus on a diode's internal thermoelectric cooling rather than its use in thermoelectric power generation, as the latter application has been shown to be quite limited.[8,9]

4.5.1 p–n Junction: Zero Bias

At zero bias, a p–n junction's drift and diffusion currents balance. Drifting carriers are accelerated by the built-in field and deposit heat energy in the lattice, while diffusing carriers remove heat energy thermoelectrically from the lattice in surmounting the built in field. These two effects cancel out, and the junction temperature remains constant.

The Peltier coefficient is expected to have a sharp discontinuity at the p–n junction because the majority carrier concentration decreases dramatically in the depletion region and then suddenly switches polarity. This has the effect of increasing the magnitude of π and then suddenly switching its sign.

A self-consistent solution to the drift-diffusion equations and Poisson's equation can be used to plot the band structure and carrier concentration of a given diode, as shown in Figure 4.4a and Figure 4.4b. The spatial variation of the total Peltier coefficient, and hence the spatial variation of the total Seebeck coefficient $\alpha = \pi/T$, can then be calculated using Equation 4.2. Figure 4.4c shows a scanning thermoelectric microscopy measurement of the thermoelectric voltage $\alpha\Delta T$ caused by a temperature difference ΔT, applied between the unbiased p–n junction and a probe tip.[10] Here the calculated thermoelectric voltage has been convolved with a Gaussian function of radius equal to that of the probe tip. It may be noted that the effect of minority carriers increases the Peltier coefficient to a value much higher than the bulk value, which has implications for microscale cooling.

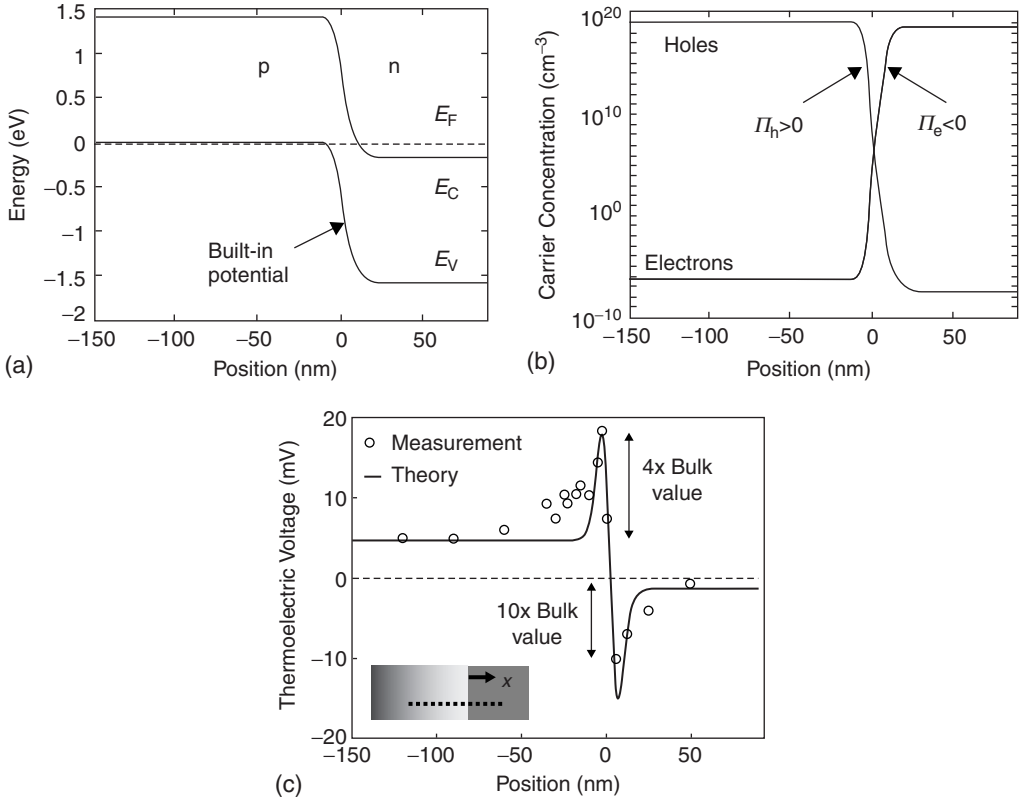

FIGURE 4.4 Unbiased GaAs p–n junction with $N_A = 1 \times 10^{19}$ and $N_D = 5 \times 10^{18}$: (a) calculated band structure; (b) calculated carrier concentration; and (c) measurement of thermoelectric voltage using scanning thermoelectric microscopy.[10]

4.5.2 p–n Junction: Forward Bias

As a bias V is applied and the junction's built in potential V_{bi} is lowered, the diffusion current grows much larger than the drift current, and overall thermoelectric cooling occurs at the junction. The thermoelectric effects of electrons and holes at the junction can be superimposed to yield the total junction cooling power density

$$Q_j = J_h(\pi_{n,h} - \pi_{p,h}) - J_e(\pi_{p,e} - \pi_{n,e}) \approx J(V_{bi} - V) \tag{4.8}$$

where J is the total current density.

In the limit of short semiconductor regions or long recombination lengths, and assuming Ohmic contacts, injected minority carriers travel from the junction to the contacts and then recombine to release the heat which was absorbed at the junction during a complementary thermoelectric heating process. In this limit, and assuming that the contacts are held at a common temperature by perfect heatsinks, the maximum temperature difference which can be obtained between the junction and the contacts can be approximated by[9]

$$\Delta T_{max} = \frac{(k_B T_j)^2 \mu n_n}{\exp(1)^* e\kappa} \tag{4.9}$$

where $\mu \approx \mu_e$ is the overall mobility, $n_n = p_p$ is the (symmetric) doping concentration, and κ is the total thermal conductivity. As an example, $In_{0.53}Ga_{0.47}As$ (a common III–V semiconductor in

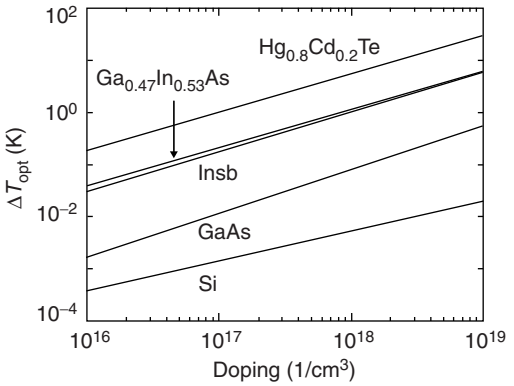

FIGURE 4.5 Maximal temperature drop due to internal thermoelectric cooling in a diode for several material systems, calculated using Fermi–Dirac statistics and assuming ideal Ohmic contact heatsinks.[7]

optoelectronic devices) with $n_n = 1 \times 10^{18}$ cm^{-3} has $\mu \approx 5000$ cm^2/Vs[11] and $\kappa \approx 0.05$ W/mK,[12] giving $\Delta T_{max} \approx 4$ K at $T_j = 300$ K. While the derivation of Equation 4.9 assumes Boltzmann statistics, numerical corrections using Fermi–Dirac statistics indicate that ΔT_{max} will be in the order of 10 K for degenerately-doped $In_{0.53}Ga_{0.47}As$, and even higher for materials such as, $Hg_{0.8}Cd_{0.2}Te$.[7] Although this does not correspond to a large thermoelectric figure-of-merit relative to BiTe based Peltier coolers, an internal temperature drop of this magnitude can have a large effect on the performance of an active device (Figure 4.5).

In a real device, highly degenerate doping may lead to tunneling, although this effect diminishes at higher current densities. Also, many carriers may recombine before reaching the contacts, which themselves do not act as perfect heatsinks. In this case, recombination heating and heat conduction from the contacts will decrease the thermoelectric cooling at the junction. Materials such as $In_{0.53}Ga_{0.47}As$ can, however, have diffusion lengths of several microns at relevant doping levels.[13] Recombination may also be optical rather than nonradiative; if the external efficiency of the (light-emitting) diode is high, some amount of recombination energy will be dissipated as light rather than heat.[14,15]

4.5.3 Heterojunctions and Nonequilibrium Effects

In addition to thermoelectric effects which occur as carriers move against electric fields at homojunction diffusion barriers, such effects also occur when carriers move against electric fields at interfaces between materials. In order to apply internal thermoelectric cooling concepts to modern active devices, which are often constructed from layers of different materials, the model presented above must be extended to heterojunctions.

Solving the drift-diffusion equations self-consistently with Poisson's equation, the band structure and quasi-Fermi levels are determined as a function of bias, as illustrated for an example heterojunction diode in Figure 4.6a. The Peltier coefficients are then solved as a function of space, as shown in Figure 4.6b; because the coefficients remain roughly constant within each region for each type of carrier, spatially-averaged Peltier coefficients can be defined within each region. The left half of Equation 4.8 is then applied to determine the heat exchange at the junction, as shown in Figure 4.6d.

In the case of the homojunction diode, a built-in potential is present for all typical bias ranges, and the net thermoelectric effect at the junction is always cooling. For the heterojunction diode, the magnitude and sign of the band offsets may be enough to overcome the built in potential and cause net heating at the junction for certain ranges of bias, as illustrated at high bias levels in Figure 4.6d.

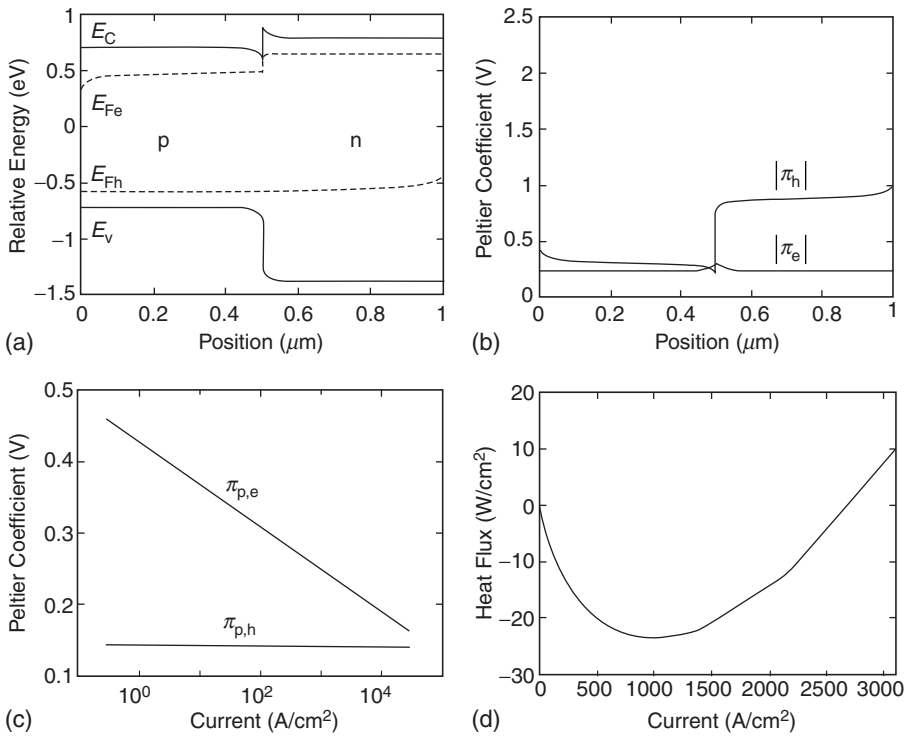

FIGURE 4.6 GaAs/AlAs heterojunction diode with $N_A = N_D = 5 \times 10^{16}$, biased at 1.25 V: (a) band structure; (b) Peltier coefficient magnitude; (c) bias dependence of Peltier coefficients in p-type region; and (d) bias dependence of thermoelectric heat exchange at the junction.[16]

The heterojunction case motivates a discussion of the distinction between equilibrium and nonequilibrium thermal effects, as the latter tend to occur at small spatial scales near sharp interfaces. Thermionic cooling, for example, is specifically based on the flow of carriers between nonequilibrium distributions.[17,18] Thermoelectric cooling, on the other hand, is by definition a quasi-equilibrium process and it describes the flow of carriers between near-equilibrium distributions. While thermionic emission effects are expected to take place in the traditional Peltier cooler at metal–semiconductor junctions, the nonequilibrium nature of the carrier distributions near the junctions is not taken into consideration in thermoelectric theory. Instead, only average energy shifts between "bulk" equilibrium distributions some distance away from the interface are considered, such as above, where the Peltier coefficient has been spatially averaged within each semiconductor region. Nonequilibrium effects which occur at very small spatial scales (where temperature may not be well defined) are not described here; thermoelectric energy transfer is simply assumed to take place somewhere in the vicinity of the junction. In profiling the spatial variation of the Peltier coefficient in devices, which may have very thin layers, the spatial average approximation will begin to break down as layer thicknesses become less than the carrier energy relaxation length.

In order to examine the regimes of device operation for which this will take place, a discussion of hot carrier effects is warranted. These effects are important in regions of large electric field or high current density, where carriers can be out of equilibrium with the lattice. The strength of the coupling between electron and phonon systems sets the difference between the electron temperature T_e and the lattice temperature T_l and also governs the length scale over which these temperatures differ.

Under steady-state conditions, the energy balance derived from the one-dimensional Boltzmann transport equation, using the displaced Maxwellian approximation, leads to the following coupled

equations for electron and lattice temperatures[5]:

$$-\kappa_e \frac{d^2 T_e}{dx^2} + G(T_e - T_l) = J\varepsilon - Q_{TE} \tag{4.10a}$$

$$-\kappa_l \frac{d^2 T_l}{dx^2} + G(T_l - T_e) = 0 \tag{4.10b}$$

where κ_e and κ_l are the respective electron and lattice thermal conductivities, G is a coupling constant for energy transfer between electrons and phonons, Q_{TE} is the thermoelectric cooling term, and ε is the x component of an accelerating electric field acting on electron current J.

Thermoelectric effects are typically strongest in a heavily-doped structures, which minimize Joule heating and (as in the case of the diode) have large built in potentials applied over narrow junction regions. Here, it is appropriate to approximate $E \approx 0$ and $Q_{TE} = J\Phi\delta(x - x_j)$ where x_j is the junction location and Φ is the potential barrier. The coupling term can be expressed by $G = \dfrac{3nk_B}{2\tau_E}$, where n is the electron concentration and τ_E is the electron energy relaxation time.[5]

The solution to Equation 4.10a and Equation 4.10b is dependent on imposed boundary conditions, but an approximate length scale L, over which electrons and phonons are expected to be out of equilibrium, can be derived[19] by assuming that the solutions of T_e and T_l are of the form $e^{-x/L}$:

$$\frac{1}{L^2} \approx G\frac{\kappa_e + \kappa_l}{\kappa_e \kappa_l} \tag{4.11}$$

Assuming worst case values, an $In_{0.53}Ga_{0.47}As$ diode with $n = 10^{19}$ cm^{-3}, $\kappa_l = 0.05$ W/cm K, $\kappa_e = 0.005$ W/cm K, and $\tau_E = 1$ ps[20–22] yields $G = 2 \times 10^8$ W/cm^3 K and $L = 50$ nm, implying that electron and lattice temperatures will equilibrate at most only 50 nm from the junction. The complete transfer of heat is expected to occur in close proximity to the junction; further reduction of the relaxation length is expected from electron-hole scattering, which can be on the same order as electron–phonon scattering.[23,24]

4.5.4 Heterostructure Devices

The thermoelectric model developed above to describe p–n junctions and heterojunctions can now be extended to profile thermoelectric heat exchange which takes place inside more complicated active devices such as those made up of heterostructures, constructed from many layers of different materials to customize material properties for device performance.

Figure 4.7 shows a GaSb-based separate confinement heterostructure (SCH) diode laser.[25] The spatial variation of the Peltier coefficient is shown in Figure 4.7b, and the thermoelectric heat exchange for each type of carrier at each junction can be found by multiplying the respective carrier current (shown in Figure 4.7c) by the Peltier coefficient difference across the junction. This yields the distribution of the internal thermoelectric heat exchange terms for the device, which can be incorporated into a further thermal model which includes terms such as Joule heating and nonradiative recombination to predict the temperature profile of the device.

Once the thermoelectric distribution inside a device is modeled, design improvements can be made based on optimization of internal thermoelectric effects, as illustrated in Figure 4.8 for an SCH diode laser. The performance of a diode laser is critically tied to the temperature of its quantum well, which is the material with the lowest bandgap at the center of the device. Injection currents lead to thermoelectric heating in the conventional device (shown in Figure 4.8a) at the core–cladding interfaces on either side of the quantum well. Through a rearrangement of the laser's band structure (via incorporating Type-II heterojunctions or increasing cladding doping), the core–cladding interfaces can instead cause thermoelectric cooling, as shown in Figure 4.8b. In effect, thermoelectric cooling has been moved from the edges of the device to the vicinity of the quantum well, and the complementary thermoelectric heating has been moved to the edges of the device, from where it is more easily conducted away.[26]

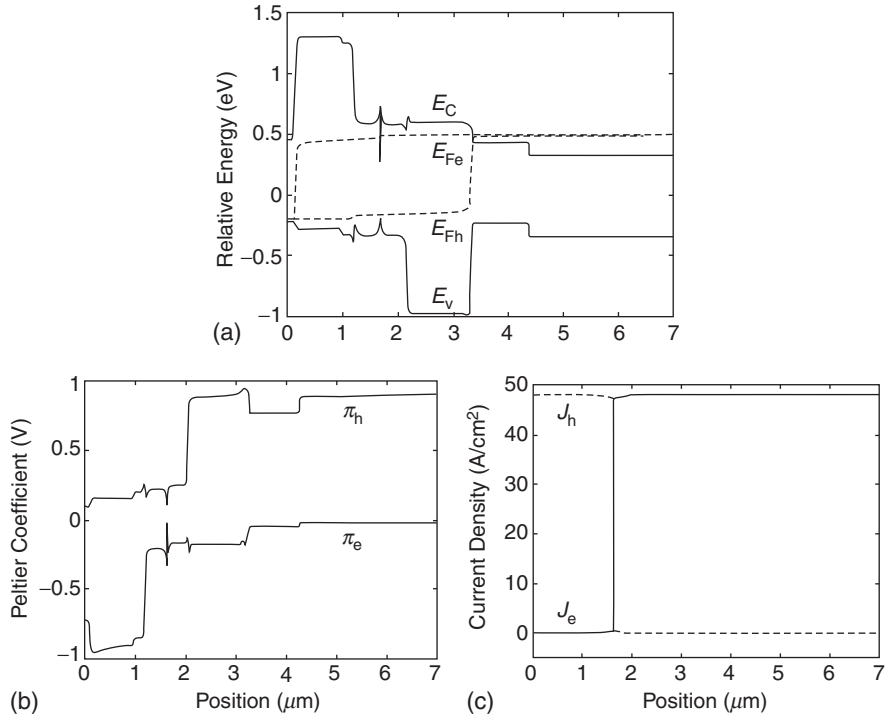

FIGURE 4.7 GaSb-based diode laser biased at 0.7 V: (a) band structure; (b) Peltier coefficients; and (c) carrier currents.[25]

Internal thermoelectric cooling is present in other devices; for example, Figure 4.9 shows cooling which takes place upon electron injection from the emitter into the base of a heterojunction bipolar transistor. While thermoelectric cooling of this sort has been modeled, very little work has been done to optimize its magnitude.

In general, internal thermoelectric effects can be large inside a heterostructure device because offsets in energy at heterojunctions can be on nearly the same order as the voltage bias of the device; the

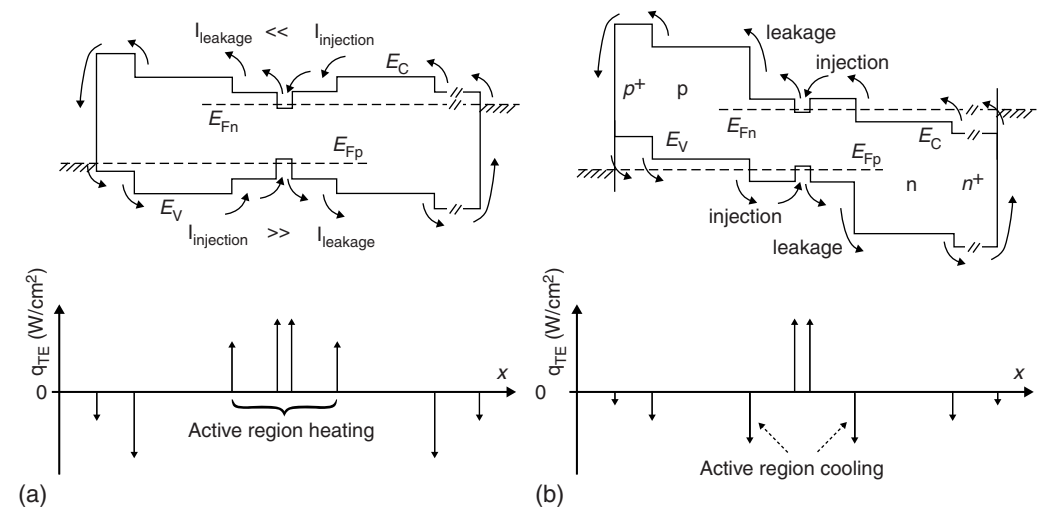

FIGURE 4.8 Internal cooling of a semiconductor laser diode: (a) conventional; and (b) internally cooled device.[26]

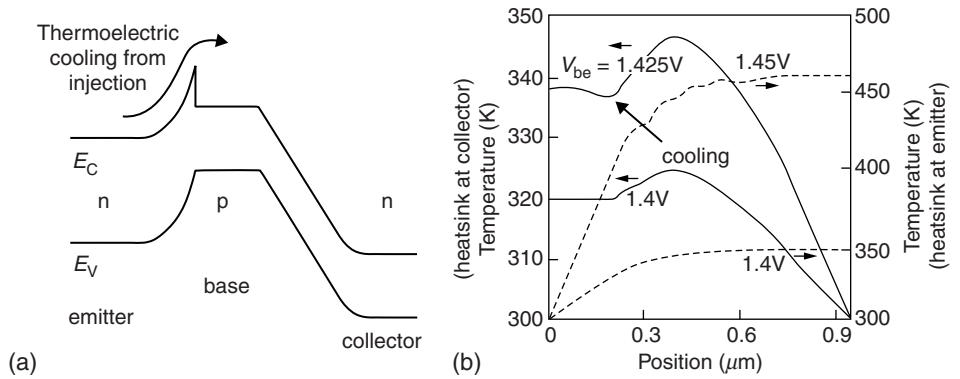

FIGURE 4.9 Internal thermoelectric cooling in a heterojunction bipolar transistor: (a) band structure; and (b) internal temperature simulation for two different boundary conditions. Solid line — heatsink at collector; dashed line — heatsink at emitter.[27]

thermoelectric heat exchange at the junctions can be nearly as great as the electrical power biasing the device. These effects are expected to be especially important in low-bandgap devices, for which band offsets can be on the same order as the bandgap, implying that thermoelectric effects can be on the same order as recombination heating.

References

1. Nakwaski, W., The Peltier coefficient in degenerate and nondegenerate semiconductors, *Electron. Technol.*, 14, 81, 1983.
2. Tauc, J., *Photo and Thermoelectric Effects in Semiconductors*, Pergamon, New York, 1956.
3. Goldsmid, H.J., *Electronic Refrigeration*, Pion, London, 1986.
4. Sah, C.-T., *Fundamentals of Solid-State Electronics*, World Scientific, New Jersey, 1991.
5. Lundstrom, M., *Fundamentals of Carrier Transport*, Cambridge University Press, New York, 2000.
6. Sze, S.M., *Physics of Semiconductor Devices*, Wiley, New York, 1981.
7. Pipe, K.P., Ram, R.J., and Shakouri, A., Bias-dependent Peltier coefficient and internal cooling in bipolar devices, *Phys. Rev. B*, 66, 125316, 2002.
8. Cutler, M., Thermoelectric behavior of p–n junctions, *J. Appl. Phys.*, 32, 222, 1961.
9. Hall, R.N., An analysis of the performance of thermoelectric devices made from long-lifetime semiconductors, *Solid-state Electron.*, 2, 115, 1961.
10. Lyeo, H.-K., Khajetoorians, A.A., Shi, L., Pipe, K.P., Ram, R.J., Shakouri, A., and Shih, C.K., Profiling the thermoelectric power of semiconductor junctions with nanometer resolution, *Science*, 303, 816, 2004.
11. Jackson, S.L., Fresina, M.T., Baker, J.E., and Stillman, G.E., High-efficiency silicon doping of InP and $In_{0.53}Ga_{0.47}As$ in gas source and metalorganic molecular beam epitaxy using silicon tetrabromide, *Appl. Phys. Lett.*, 64, 2867, 1994.
12. Paine, B.M., Shah, A.P., and Rust, T. III, The effects of ternary alloys on thermal resistance of HBTs, HEMTs, and laser diodes, *Microelectron. Rel.*, 43, 853, 2003.
13. Ambrée, P., Gruska, B., and Wandel, K., Dependence of the electron diffusion length in p-InGaAs layers on the acceptor diffusion process, *Semicond. Sci. Technol.*, 7, 858, 1992.
14. Nakwaski, W., Optical refrigeration in light-emitting diodes, *Electron. Technol.*, 13, 61, 1982.
15. Gauck, H., Gfroerer, T.H., Renn, M.J., Cornell, E.A., and Bertness, K.A., External radiative quantum efficiency of 96% from a GaAs/GaInP heterostructure, *Appl. Phys. A*, 64, 143, 1997.

16. Pipe, K.P., Ram, R.J., and Shakouri, A., Bias-dependent Peltier coefficient in bipolar devices. In *Proceedings of the ASME Heat Transfer Division*, Vol. 7, Y. Jaluria, ed., p. 219. ASME, New York, 2001.
17. Mahan, G.D., Thermionic refrigeration, *J. Appl. Phys.*, 76, 4362, 1994.
18. Shakouri, A. and Bowers, J.E., Heterostructure integrated thermionic coolers, *Appl. Phys. Lett.*, 71, 1234, 1997.
19. Zeng, T. and Chen, G., Nonequilibrium electron–phonon interaction in thin-film thermionic structures, *Proceedings of 18th International Conference on Thermoelectrics*, Baltimore, August, 1999.
20. Thobel, J.L., Baudry, L., Cappy, A., Bourel, P., and Fauquembergue, R., Electron transport properties of strained $In_xGa_{1-x}As$, *Appl. Phys. Lett.*, 56, 346, 1990.
21. Tsai, C.-Y., Tsai, C.-Y., Lo, Y.-H., and Eastman, L.F., Carrier energy relaxation time in quantum-well lasers, *IEEE J. Quant. Elect.*, 31, 2148, 1995.
22. Huxtable, S.T., et al., Thermal conductivity of indium phosphide based superlattices, *Microscale Thermophys. Eng.*, 4, 197, 2000.
23. Rodrigues, R., Juen, S.A., Lamprecht, K.F., and Höpfel, R.A., Electron-hole scattering in highly doped p-GaAs after femtosecond optical excitation, *Semicond. Sci. Technol.*, 9, 456, 1994.
24. Tsai, C.-Y., et al., Effects of electron-hole energy transfer on the nonlinear gain coefficients in the small-signal modulation response of semiconductor lasers, *Appl. Phys. Lett.*, 71, 1747, 1997.
25. Pipe, K.P., Ram, R.J., Goyal, A.K., and Turner, G.W., Electrical and thermal analysis of heat flow in $\lambda = 2.05\ \mu$m GaInAsSb/AlGaAsSb lasers, *Proceedings of Conference on Lasers and Electro-Optics*, Baltimore, June, 2003.
26. Pipe, K.P., Ram, R.J., and Shakouri, A., Internal cooling in a semiconductor laser diode, *IEEE Phot. Tech. Lett.*, 14, 453, 2002.
27. Zhou, W.Y., Liou, Y.B., and Huang, C., Steady-state and transient heat responses in AlGaAs/GaAs HBTs, *Solid-state Elect.*, 38, 1118, 1995.